

HARD VIEW SELECTION FOR SELF-SUPERVISED LEARNING

Fabio Ferreira ^{*†}

Ivo Rapant ^{*†}

Frank Hutter [†]

ABSTRACT

Many Self-Supervised Learning (SSL) methods train their models to be invariant to different “views” of an image and considerable efforts were directed towards improving pre-text tasks, architectures, or robustness. However, most SSL methods remain reliant on the random sampling of operations within the image augmentation pipeline, such as the random resized crop operation. We argue that the role of the view generation and its effect on performance has so far received insufficient attention. To address this, we propose an easy, learning-free, yet powerful Hard View Selection (HVS) strategy designed to extend the random view generation to expose the pretrained model to harder samples during SSL training. It encompasses the following iterative steps: 1) randomly sample multiple views and create pairs of two views, 2) run forward passes for each view pair on the currently trained model, 3) adversarially select the pair yielding the worst loss depending on the current model state, and 4) run the backward pass with the selected pair. As a result, HVS consistently achieves accuracy improvements between 0.91% and 1.93% on ImageNet linear evaluation and similar improvements on transfer tasks across DINO, SimSiam, iBOT and SimCLR. We provide studies to shed light on the inner workings and show that, by naively using smaller resolution images for the selection step, we can significantly reduce the computational overhead while retaining performance. Surprisingly, even when accounting for the computational overhead incurred by HVS, we achieve performance gains between 0.52% and 1.02% and closely rival the 800-epoch DINO pretraining with only 300 epochs.

1 INTRODUCTION

Various approaches to learn effective and generalizable visual representations in Self-Supervised Learning (SSL) exist. One way to categorize many SSL methods is to distinguish generative and discriminative approaches. While generative methods aim at generating image input, discriminative methods, with contrastive learning (Hadsell et al., 2006; He et al., 2020) being the most renowned approach, aim at learning a latent representation in which similar image views are closely and dissimilar ones are distantly located.

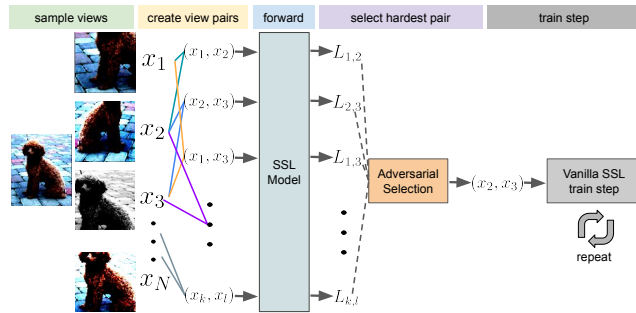


Figure 1: HVS first samples N views, pairs them, and adversarially selects the hardest pair, i.e., the one with the worst loss according to the current model state.

Such views are generated by applying a sequence of (randomly sampled) image transformations and are usually composed of geometric (cropping, rotation, etc.) and appearance (color distortion, blurring, etc.) transformations. A body of literature (Chen et al., 2020a; Wu et al., 2020; Purushwalkam & Gupta, 2020; Wagner et al., 2022; Tian et al., 2020b) has illuminated the effects of image views on representation learning and identified *random resized crop* (RRC) transformation, which

^{*}Denotes equal contribution. Correspondence to: Fabio Ferreira <ferreira@cs.uni-freiburg.de>.

[†]University of Freiburg

randomly crops the image and resizes it back to a fixed size, as well as color distortion as one of the most essential ones for effective contrastive learning. However, despite this finding and to our best knowledge, little research has gone into identifying more effective ways for *selecting* or generating views to improve performance. In this paper, we seek to extend the random view generation to expose the pretrained model to harder samples during CL training.

Supervised Learning works that address this shortcoming and which attempt to leverage task difficulty include Spatial Transformer Networks (Jaderberg et al., 2015) and Adversarial AutoAugment (Zhang et al., 2020), which either directly learn geometric transformations or generate augmentation policies that yield hard samples. However, these approaches have not been used successfully for unsupervised learning and Adversarial AutoAugment does not include RRC in its search space. In contrast to what we propose, integrating any of these methods into existing self-supervised learning pipelines is non-trivial.



Figure 2: Examples (left) and sampled views (right) after resizing and appearance transformations. Pairs selected by HVS are shown with a solid frame.

Related SSL approaches exist that aim at controlling view hardness through adversarial Shi et al. (2022); Tamkin et al. (2021) or cooperative Hou et al. (2023) models. A work that takes a similar perspective like us in leveraging the information content of views for SSL is (Tian et al., 2020b). They discover sweet spots for data augmentation hyperparameters that are widely used and adversarially learn flow-based models that generate novel color space-views which are then used for contrastive learning. While these works offer important insights into view optimality, they usually require learning additional models prior to the actual SSL training or non-trivial changes to the pipeline and thus, are not easily integrated into existing SSL methods.

In contrast, we propose a fully learning-free and easy-to-integrate approach. Importantly, and different to Tian et al. (2020b), our approach leverages the current model state and operates on a per-sample basis during pretraining. It applies the following simple strategy: we sample a few views and forward each pair through the currently trained model. Next, we identify the pair that yields the worst loss among all pairs, use it for the backward pass, and repeat (see Fig. 1). While being agnostic to any contrastive and non-contrastive loss, this strategy exposes the pretrained model to samples that the model at any given point in the training trajectory finds challenging. As our results show, sampling only four views are sufficient to achieve noticeable improvements.

Overall, our contributions can be summarized as follows:

- We propose *Hard View Selection (HVS)*, a new learning method complementing SSL that is easy to integrate and extends the broadly-used random view generation to automatically expose the model to harder samples during pretraining. The only requirement of HVS is that it needs to be able to compute sample-wise losses;
- We demonstrate the effectiveness and compatibility of our approach using ImageNet (Deng et al., 2009) pretraining across popular and widely-adopted SSL methods that cover a diverse range of objectives such as SimSiam (Chen & He, 2021), DINO (Caron et al., 2021), iBOT (Zhou et al., 2021), and SimCLR (Chen et al., 2020a);
- HVS improves all baselines noticeably compared to using the common view generation, and we show this on a diverse set of transfer datasets and tasks, including linear evaluation, finetuning, object detection and segmentation;
- We present insights into the underlying mechanisms of HVS such as the effect of changing the number of sampled views or color augmentation.

We make our PyTorch (Paszke et al., 2019) code, models, and all used hyperparameters publicly available under <https://anonymous.4open.science/r/hard-view-selection/>.

2 RELATED WORK

2.1 CONTRASTIVE AND NON-CONTRASTIVE LEARNING IN SSL

The core idea behind the contrastive learning framework is to learn image representations by contrasting positive pairs (two views of the same image) against negative pairs (two views of different images) (Hadsell et al., 2006). To work well in practice and to prevent model collapse, contrastive learning methods often require a large number of negative samples (Wu et al., 2018; van den Oord et al., 2018; Chen et al., 2020a; He et al., 2020; Tian et al., 2020a; Chen et al., 2020b) stored in memory banks (Wu et al., 2018; He et al., 2020) or, for instance, in the case of SimCLR, implicitly in large batches (Chen et al., 2020a). Non-contrastive approaches, such as BYOL (Grill et al., 2020), SimSiam (Chen & He, 2021), DINO (Caron et al., 2021) and others (Zbontar et al., 2021; Caron et al., 2020; Ermolov et al., 2021), are able to only use positive pairs without causing model collapse but rely on other techniques, such as Siamese architectures, whitening of embeddings, clustering, maximizing the entropy of the embeddings, momentum encoders, and more.

2.2 OPTIMIZING FOR HARD AUGMENTATIONS AND VIEWS IN SSL

Past work has shown that optimizing augmentation policies or views directly can be beneficial. Hence, the realm of learning task-specific augmentation policies based on data has seen quick development (Cubuk et al., 2019; Ho et al., 2019; Lin et al., 2019; Zhang et al., 2020; Hataya et al., 2020; Müller & Hutter, 2021). Most related to our work among these approaches is Adversarial AutoAugment (AAA) (Zhang et al., 2020) that proposes to generate augmentation policies yielding hard samples by learning with an adversarial supervised objective. In a similar, but cooperative setting, MADAug (Hou et al., 2023) learns policies yielding progressively harder samples. In contrast to our work, however, AAA and MADAug do not include the random resize crop operation into their search spaces and thus, are limited in leveraging the geometric perspective to control view hardness.

Unlike learning hard augmentations, approaches exist that optimize directly on the pixel level to control view hardness. For instance, Shi et al. (2022) adversarially learn semantically meaningful masks for a pretrained network to inpaint. Another approach perturbs input images using an adversarial model (Tamkin et al., 2021). Tian et al. (2020b) leverage, like us, the view content for better performance. Under the lens of mutual information (MI), they derive an objective to adversarially learn flow-based view generators for contrastive learning. While these methods can complement our approach, they are less easily integrated into existing contrastive pipelines due to the need for adversarial network training. Moreover, Tian et al. (2020b) does not use the current model state to control learning hardness and, while their studies incorporate distance metrics, they do not consider the Intersection over Union (IoU) metric which we extensively make use of.

3 METHOD

3.1 CONTRASTIVE LEARNING FRAMEWORK

In this section, we introduce our approach which is also depicted in Algorithm 1. Many different contrastive learning (He et al., 2020) objectives exist, each characterized by variations stemming from design choices, such as by the use of positive and negative samples or asymmetry in the encoder-projector network structure. For simplicity of exposure, we will introduce our approach based on the SimSiam objective Chen & He (2021), but we do note that our method can be used with any other discriminative SSL objective that allows the computation of a sample-wise losses.

SimSiam works as follows. Assume a given set of images \mathcal{D} , an image augmentation distribution \mathcal{T} , a minibatch of M images $\mathbf{x} = \{x_i\}_{i=1}^M$ sampled uniformly from \mathcal{D} , and two sets of randomly sampled image augmentations A and B sampled from \mathcal{T} . SimSiam applies A and B to each image in \mathbf{x} resulting in \mathbf{x}^A and \mathbf{x}^B . Both augmented sets of views are subsequently projected into an embedding space with $\mathbf{z}^A = g_\theta(f_\theta(\mathbf{x}^A))$ and $\mathbf{h}^B = f_\theta(\mathbf{x}^B)$ where f_θ represents an encoder (or backbone) and g_θ a projector network. SimSiam then minimizes the following objective:

$$\mathcal{L}(\theta) = \frac{1}{2} (D(\mathbf{z}^A, \mathbf{h}^B) + D(\mathbf{z}^B, \mathbf{h}^A)) \quad (1)$$

where D denotes the negative cosine similarity function. Intuitively, when optimizing θ , the embeddings of the two augmented views are attracted to each other.

3.2 HARD VIEW SELECTION

As previously described, Hard View Selection extends the random view generation by sampling adversarially harder views during pretraining. Instead of having two sets of augmentations A and B , we now sample N sets of augmentations, denoted as $\mathcal{A} = \{A_1, A_2, \dots, A_N\}$. Each set A_i is sampled from the image augmentation distribution \mathcal{T} , and applied to each image in \mathbf{x} , resulting in N augmented sets of views $\mathbf{x}^{A_1}, \mathbf{x}^{A_2}, \dots, \mathbf{x}^{A_N}$. Similarly, we obtain N sets of embeddings $\mathbf{z}^{A_1}, \mathbf{z}^{A_2}, \dots, \mathbf{z}^{A_N}$ and predictions $\mathbf{h}^{A_1}, \mathbf{h}^{A_2}, \dots, \mathbf{h}^{A_N}$ through the encoder and projector networks. We then define a new objective function that seeks to find the pair $(x_i^{A_k}, x_i^{A_l})$ of a given image x_i that yields the highest loss:

$$(x_i^{A_k}, x_i^{A_l}) = \arg \max_{k,l;k \neq l} \mathcal{L}(\theta)_{i,k,l} = \arg \max_{k,l;k \neq l} \frac{1}{2} \left(D(z_i^{A_k}, h_i^{A_l}) + D(z_i^{A_l}, h_i^{A_k}) \right), \quad (2)$$

where $\mathcal{L}(\theta)_{i,k,l}$ simply denotes a sample-wise variant of Eq. 1. Overall, we first generate N augmented views for each image x_i in the minibatch. Then, we create all combinatorially possible $\binom{N}{2}$ pairs of augmented images for x_i . Then, we use Eq. 2 to compute the sample-wise loss for each pair which corresponds to invoking forward passes. We then select all pairs that yielded the highest loss to form the new *hard* minibatch of augmented sets $\mathbf{x}^{A_{k^*}}$ and $\mathbf{x}^{B_{l^*}}$, discard the other pairs and use the hard minibatch for optimization.

As shown in Algorithm 1, we repeat this process in each training iteration. This modification introduces a more challenging learning scenario in which the model is encouraged to learn more discriminative features by being exposed to harder views. While the additional forward passes come with a certain overhead (about a factor of $1.55\times$ for SimSiam), as we will demonstrate in our experiments, the focus on harder views leads to consistent improvements.

While we exemplified the integration of HVS with the SimSiam objective, integrating it into other contrastive

methods is as straightforward. The only requirement of HVS is to be able to compute sample-wise losses (in order to select the views with the highest loss). In our experiments section and in addition to SimSiam, we study the application of HVS to the objectives of DINO and SimCLR (see also Appendix I.1 for a formal exemplary definition for the integration of HVS into SimCLR).

3.3 IMPLEMENTATION AND EVALUATION PROTOCOLS

Implementation We now describe the technical details of our approach. HVS can be used with any contrastive method that allows computing sample-wise losses, and the only two elements in the pipeline we adapt are: 1) the data loader (needs to sample N views for each image) and 2) the forward pass (invokes the *select* function to identify and return the hard views). The image transformation distribution \mathcal{T} of the baselines is left unchanged. Note, for the view selection one could simply resort to RRC only and apply the rest of operations after the hard view selection (see Section 5.1 for a study on the influence of appearance on the selection). All experiments were conducted with $N = 4$ sampled views, yielding $\binom{N}{2} = 6$ pairs to compare, except for DINO that uses 10 views (2 global, 8 local heads) per default. For DINO, we apply HVS to both global and local heads but to remain tractable, we upper-bound the number of total pair comparisons to 128. SimCLR uses positive and negative samples. In accordance with the simplicity of HVS, we do not

Algorithm 1 Contrastive Learning with HVS

- 1: **Input:** Number of views $N \geq 2$, batch size M ,
 - 2: augmentation distribution \mathcal{T} , encoder f_θ , projector g_θ
 - 3: **for** each x_i in the sampled minibatch $\{x_i\}_{i=1}^M$ **do**
 - 4: Sample N augmentations: $A = \{t_n \sim \mathcal{T}\}_{n=0}^N$
 - 5: Create augmented views: $\mathbf{x}_i^A = \{t_n(x_i)\}_{n=0}^N$
 - 6: Forward all views through f_θ and g_θ to get z and h
 - 7: Create all $\binom{N}{2}$ possible pairs $\mathbf{x}_i^{A_k} \times \mathbf{x}_i^{A_l}, k \neq l$
 - 8: Select the *hard* pair $(x_i^{A_{k^*}}, x_i^{A_{l^*}})$ maximizing Eq. 2
 - 9: Create the minibatch $(\mathbf{x}^{A_{k^*}}, \mathbf{x}^{A_{l^*}})$ consisting of hard pairs
 - 10: Proceed with standard contrastive learning training to update θ with the hard batch
 - 11: Repeat for all minibatches
 - 12: **return** Optimized θ
-

alter its objective, which naturally leads to selecting hard views that are adversarial to positive and “cooperative” to negative views.

Evaluation Protocols We now describe the protocols used to evaluate the performance in our main results section. In self-supervised learning, it is common to assess pretraining performance with the linear evaluation protocol by training a linear classifier on top of frozen features or finetuning the features on downstream tasks. Our general procedure is to follow the baseline methods as closely as possible, including hyperparameters and code bases (if reported). It is common to use RRC and horizontal flips during training and report the test accuracy on central crops. Due to the sensitivity of hyperparameters, and as done by Caron et al. (2021), we also report the quality of features with a simple weighted nearest neighbor classifier (k-NN).

Method	Arch.	100 epochs		300 epochs	
		Lin.	k-NN	Lin.	k-NN
DINO	ViT-S/16	73.52	68.80	75.48	72.62
+ HVS	ViT-S/16	74.67	70.72	76.56	73.64
Improvement		+1.15	+1.92	+1.08	+1.02
DINO	RN50	71.93	66.28	75.25	69.53
+ HVS	RN50	72.87	67.33	75.65	70.05
Improvement		+0.94	+1.05	+0.40	+0.52
SimSiam	RN50	68.20	57.47	70.35	61.40
+ HVS	RN50	68.98	58.97	70.90	62.97
Improvement		+0.78	+1.50	+0.55	+1.57
SimCLR	RN50	63.40	52.83	65.50	55.65
+ HVS	RN50	65.33	54.76	67.20	57.31
Improvement		+1.93	+1.85	+1.70	+1.66
iBOT	ViT-S/16	69.50	62.82	72.48	66.60
+ HVS	ViT-S/16	70.41	63.05	73.99	67.12
Improvement		+0.91	+0.23	+1.51	+0.52

4 MAIN RESULTS

Here, we discuss our main results on image classification, object detection, and segmentation tasks. All results are self-reproduced using the baseline code and available hyperparameters, and are averaged over 3 seeds (iBOT over 2 seeds). All hyperparameters are reported in Appendix G.

Table 1: Average top-1 linear and k-NN classification accuracy on the ImageNet validation set for 100 and 300-epoch pretrainings. For SimCLR we run 200 instead of 300 epochs.

4.1 EVALUATIONS ON IMAGENET

We report the top-1 validation accuracy on frozen features, as well as the k-NN classifier performance, in Table 1. For DINO, we additionally compare ResNet-50 (He et al., 2016) against the ViT-S/16 (Dosovitskiy et al., 2020) architecture. Our method compares favourably against all baselines with an increased performance of approximately 1% on average, showing the benefit of sampling hard views. We highlight that our 300-epoch DINO+HVS model exhibits strong performance, closely rivaling the officially reported 800-epoch DINO performance of 77%, with a mere $\sim 0.4\%$ performance gap. This achievement remains favorable, even when factoring in the $2\times$ slowdown (DINO with 2 global, 8 local heads) induced by our method. Due to limited compute resources, we run the pretrainings for 100 and 300 epochs (200 epochs for SimCLR) and batch sizes of 512 (100 epoch) or 1024 (200 & 300 epoch trainings), respectively. This choice is in line with a strategy that favors the evaluation of a diverse and larger set of baselines over the evaluation of a less diverse and smaller set and underpins the broad applicability of HVS. We primarily ran our experiments with 8xNVIDIA GeForce RTX 2080 Ti nodes, with which the cheapest runs required ~ 3.5 days for pretraining and linear evaluation and the most expensive runs required ~ 25 days. Moreover, we emphasize that HVS is insensitive to the baseline hyperparameters and simply reusing these consistently resulted in improvements of the reported magnitudes across all experiments.

4.2 TRANSFER TO OTHER DATASETS AND TASKS

We now demonstrate the transferability of features learned with HVS. For all transfer experiments, we use our 100-epoch ImageNet pretrained SimSiam ResNet-50 and DINO ViT-S/16 models.

Linear Evaluation and Finetuning In Table 2, we apply both the linear evaluation (Lin.) and finetuning (FT.) protocols to our models across a diverse set of datasets consisting of CIFAR10 Krizhevsky (2009), CIFAR100, Flowers102Nilsback & Zisserman (2008), Food101Bossard et al. (2014), and iNaturalist 2021 (iNaturalist 2021 competition dataset). Our results show that the improvements achieved by sampling hard views we observed so far also transfer to other datasets.

Method	Arch.	CIFAR10		CIFAR100		Flowers102		iNat 21		Food101	
		Lin.	F.T.								
SimSiam	RN50	82.60	95.50	54.20	77.20	34.27	56.40	32.50	60.30	65.70	83.90
+ HVS	RN50	84.40	96.10	57.10	78.20	38.37	58.90	33.90	60.90	67.10	84.70
Improvement		+1.80	+0.60	+2.90	+1.00	+4.10	+2.50	+1.40	+0.60	+1.40	+0.80
DINO	ViT-S/16	94.53	98.53	80.63	87.90	91.10	93.20	46.93	53.97	73.30	87.50
+ HVS	ViT-S/16	95.13	98.65	81.27	88.23	92.07	93.60	49.03	54.16	74.13	87.91
Improvement		+0.60	+0.12	+0.63	+0.33	+0.97	+0.40	+2.10	+0.19	+0.83	+0.41

Table 2: Models trained on ImageNet with HVS compare favourably against models trained without it when transferred to other datasets through finetuning (F.T.) or the linear evaluation protocol (Lin.).

Object Detection and Instance Segmentation For object detection, we use the VOC07+12 (Everingham et al., 2010) dataset using Faster R-CNN (Ren et al., 2015). We study instance segmentation on the COCO (Lin et al., 2014) dataset using Mask R-CNN (He et al., 2022). Table 3, where we report the AP50 performance, shows that the features learned with HVS also mostly transfer favourably to these tasks and outperform the SimSiam baseline with a 100-ep. pretraining. However, in case of DINO, we observe a slight performance gap on the detection task, which is the only instance in the entire paper where HVS did not outperform the baseline. This result warrants further investigation, as it was conducted with a single seed (due to limited compute resources). More details and performance results on this task are provided in Appendix F.1.

Method	Arch.	VOC Det.	COCO Segm.
SimSiam	RN50	78.46	45.16
+ HVS	RN50	79.06	46.51
Impr.		+0.60	+1.35
DINO	RN50	80.86	50.35
+ HVS	RN50	80.51	50.39
Impr.		-0.36	+0.04

Table 3: AP50 for object detection and instance segmentation.

4.3 TIME COMPLEXITY OF HVS

The additional forward passes that HVS introduces for the selection phase increase the time complexity of the individual baseline methods. Several possible approaches exist to mitigate this overhead, one of which is to reduce the image resolution for the selection step (while still using the original resolution for learning). We measured the overhead factors under varying image resolutions for SimSiam and DINO and report them in Table 14 in the appendix. Given the 20% (SimSiam) to 30% (DINO) faster training times per batch when using a 50% image reduction, we evaluated this approach and observed that final performances are retained across all tested methods. Table 4 provides insights into the HVS’ performance when computational overhead is accounted for in the 50% reduction case. Overall, the results validate the effectiveness of HVS in reducing computational demands without compromising on performance. We refer to Section H in the appendix for a discussion on further optimizing HVS.

Method	Arch.	Lin.
DINO	ViT-S/16	74.06
+ HVS	ViT-S/16	74.67
Impr.		+0.61
SimSiam	RN50	68.46
+ HVS	RN50	68.98
Impr.		+0.52
SimCLR	RN50	64.31
+ HVS	RN50	65.33
Impr.		+1.02

Table 4: Accounting for computational overhead with 50% resolution (100 epochs).

5 EMPIRICAL ANALYSIS OF HARD VIEW SELECTION

In this section, we discuss studies designed to shed light on the mechanisms underlying HVS. We address the following questions: 1) “Which can be observed that underlie the hard view selection?” 2) “Can a “manual” augmentation policy be inferred from these patterns?”, and 3) “What are the effects on empowering the adversary?”. For all experiments conducted here, we use our 100-epoch, ImageNet-pretrained SimSiam+HVS models with four sampled views.

5.1 Q1: WHICH PATTERNS UNDERLYING THE HARD VIEW SELECTION CAN BE OBSERVED?

When visually studying examples and the views selected by HVS in Figures 2 and 5 (in the appendix), we notice that both geometric and appearance characteristics seem to be exploited, for

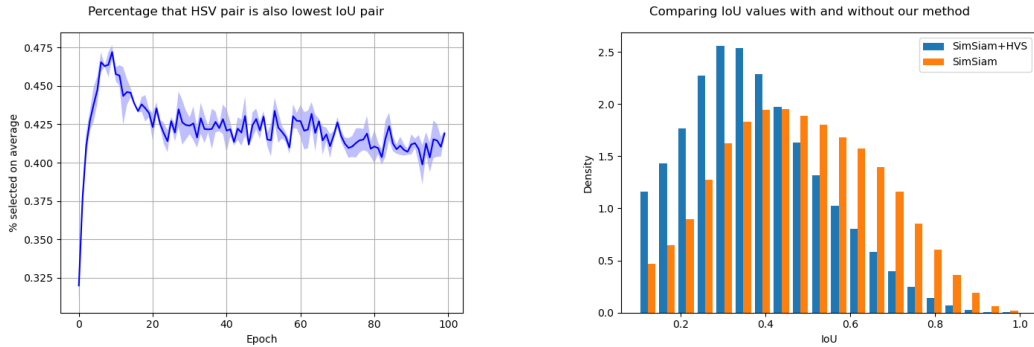


Figure 3: **Left:** In over 40% of the cases, the adversarially selected view pair is also the one with the lowest IoU throughout SimSiam+HVS pretraining. We attribute the spike in the early phase to the random initialization of the embedding. **Right:** When using HVS (blue), a shift to smaller IoU values is visible when comparing to standard pretraining (orange). Both results are based on 3 seeds.

instance, see the brightness difference between the views of the first two rows in Fig. 2. We also see a generally higher training loss (Fig. 6 in the appendix) indicative of an increased task difficulty.

Logging Augmentation Data To assess these observations, we logged relevant hyperparameter data during SimSiam training with HVS. The logs include for each view the sampled geometric and appearance parameters from the data augmentation operations (such as the height/width of the crops or the brightness; see Section D in the appendix for more details), as well as the loss and whether the view was selected. As evaluated metrics we chose the Intersection over Union (IoU), Relative Distance (normalized distance of the center points views), color distortion distance (the Euclidean distance between all four color distortion parameters), and the individual color distortion parameters.

Importance of Augmentation Metrics Given 300k such samples, we then used fANOVA (Hutter et al., 2014) to determine how predictive these metrics are. This resulted in the metric with the highest predictive capacity on the loss to be the IoU, explaining 15% of the variance in performance, followed by brightness with 5% (for more details see Fig. 8 in the appendix). The importance of IoU in HVS is further underpinned by the following observation: the fraction of view pairs selected by HVS, which are also the pairs with the lowest IoU among all six pairs ($N=4$), is over 40% (random: $\sim 16.7\%$) during training. Moreover, when using HVS, a shift to smaller IoU values can be observed when comparing against standard pretraining. We visualize both findings in Fig. 3.

Taking a Closer Look at the Intersection over Union We also examined the IoU value over the course of training in Fig. 4 (left). An observable pattern is that the IoU value with HVS (Fig. 4 (left) in blue) is smaller and varies more when compared against training without HVS (green). We believe this is due to the sample-wise and stateful nature of the adversarial selection as HVS chooses different IoU values between varying samples and model states. Lastly, we assessed the effect of the color augmentation on the pair selection. For this study, we sampled *one* set of color augmentations (as opposed to one for each view) per iteration and applied it to all views. Only after identifying the hardest pair, we apply sampled data augmentations to each view. As we show in Fig. 4 (right), the fraction of selected pairs that are also the hardest pairs slightly increases in this case. One possible explanation for this is that it reflects the non-negligible role of color variation between views (as shown previously with the importance analysis), where HVS is given less leverage to increase hardness through a static appearance and instead, depends more on leveraging the IoU. Another key observation is that HVS often chooses view pairs that incorporate zooming in and out or an increased distance between the views (see last row of Fig. 2). We believe the former relates to the analogy of local-to-global view correspondence described in SimCLR and the DINO papers.

5.2 Q2: CAN A MANUAL AUGMENTATION POLICY BE INFERRED?

Since harder pretraining tasks seem beneficial according to observations made in Q1, a natural question arises: is it possible to mimic the adversarial selection with a manually scripted augmentation policy? Such a policy would replace HVS and lower the computational cost. Since the IoU plays

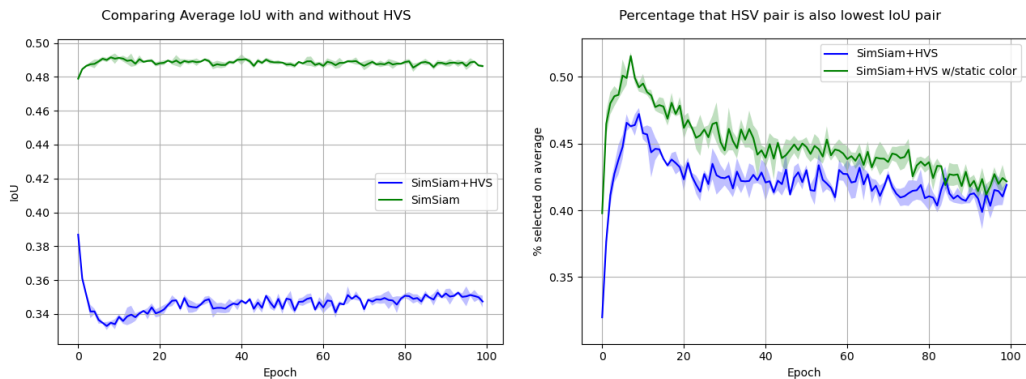


Figure 4: **Left:** The average IoU of view pairs selected by SimSiam+HVS (blue) compared against the default SimSiam training (green). **Right:** Using static color augmentation for all pairs before the selection increases the dependency on the IoU.

an important role, below, we study several possible ways for constructing a simple manual augmentation policy based on IoU.

Deriving an Augmentation Policy We implemented the following rejection sampling algorithm in the augmentation pipeline: we linearly approximate the IoU values from Fig. 4 (left; in blue) with start and end values of 0.30 and 0.35 (ignoring the dip in the early phase). For each iteration, we then check if the pairs exceed the IoU value and if so, we reject the pair and re-sample a new pair. This ensures that only pairs are sampled that entail a minimum task difficulty (by means of a small enough IoU). We varied different hyperparameters, e.g., IoU start/end ranges, inverse schedules, and alternating between the IoU schedule and the standard augmentation. Training both SimSiam and DINO models for 100 epochs yielded performance decreases or insignificant improvements (see Table 5). These results indicate that developing a manual policy based on metrics in pixel space such as the IoU is non-trivial. Additionally, these results show that transferring such a policy from SimSiam to DINO does not work well, possibly due to additional variations in the augmentation pipeline such as multi-crop. In contrast, we believe that HVS is effective and transfers well since it 1) operates on a similarity level of latent embeddings that may be decorrelated from the pixel space and 2) has access to the current model state.

IoU Policy Type	SimSiam	DINO
Baseline (B)	68.20	73.50
B+range(0.3-0.35)	-0.80	-1.47
B+range(0.3-0.35)+alt.	+0.10	-0.45
B+range(0.4-0.6)	+0.55	-0.40
B+range(0.4-0.6)+alt.	+0.25	-0.20
B+range(0.1-0.8)	-33.95	-1.50
B+range(1.0-0.1)	+0.07	-

Table 5: Top-1 lin. eval. accuracies for the manual IoU policy (averaged over 2 seeds).

Assessing the Difficulty of Predicting the Pair Selected by HVS We further validated the previous result and assess an upper limit on the performance for predicting the hardest pair. By fitting a gradient boosting classification tree (Friedman, 2001), we predict the selected view pair conditioned on all SimSiam hyperparameter log data from Q1 except for the flag that indicates whether a view was selected. As training and test data, we used the logs from two seeds (each 300k samples) and the logs from a third seed, respectively. We also tuned hyperparameters on train/valid splits and applied a 5-fold CV. However, the resulting average test performance in all scenarios never exceeded 40%, indicating that it is indeed challenging to predict the hardness of views based on parameter-level data. This further supports our hypothesis that deriving a policy for controlling and increasing hardness based on geometric and appearance parameters is non-trivial and that such a policy must function on a per-sample basis and have access to the current model state as in HVS.

5.3 Q3: WHAT ARE THE EFFECTS OF EMPOWERING THE ADVERSARY?

It is well known that adversarial learning can suffer from algorithmic instability (Xing et al., 2021), e.g. by giving an adversary too much capacity. We now further explore the space of adversarial capacity for selecting hard views to gain a better understanding of its impact on contrastive learning.

Optimizing an Adversarial Learner for the View Generation In this experiment, we briefly explore adversarially learning a network to output the transformation matrix for view generation. We optimize a Spatial Transformer Network (STN) (Jaderberg et al., 2015) jointly with the DINO objective and a ViT-tiny. Using the inverse of the DINO loss, we train the STN to output the geometric transformation matrices (each 6 parameters) for generating views. We employ and test various transformation types (e.g., rotation, translation, etc.) that influence the capacity of the adversary. We discuss this experiment in greater detail in Appendix E and briefly summarize our findings here: applying an adversary in this way is very challenging due to the sensitivity of CL on the data augmentation and the dynamics of adversarial learning, often leading to either minor improvements or model collapses as we have observed when employing a too strong manual IoU policy in Q1.

Increasing the Number of Views In our initial experiments, we explored variations in the number of sampled views N with SimSiam and HVS. As can be seen in Fig. 7 in the appendix, while $N = 8$ views still outperform the baseline in terms of linear evaluation accuracy, it is slightly worse than using $N = 4$ views (-0.05% for 100 epochs and -0.14% for 200 epochs pretraining on linear evaluation). We interpret this result as the existence of a “sweet spot” in setting the number of views, where, in the limit, a higher number of views corresponds to approximating the adversarial learner described above. This would allow HVS to select progressively harder views that quickly results in very hard tasks and consequently in model collapse and performance deterioration.¹

6 CONCLUSION

In this study, we presented HVS, a new data augmentation and learning strategy for Self-Supervised Learning designed to challenge pretrained models with more demanding samples. This method, while straightforward in its design, has proven to be a powerful tool, pushing the boundaries of the traditional random view generation in SSL. When combined with methods like DINO, SimSiam, iBOT, and SimCLR, HVS consistently showcased improvements in linear evaluation and a diverse set of transfer tasks. As the landscape of self-supervised learning continues to evolve, methods like HVS underscore the potential for further advancements in the field. By continuously challenging models with harder samples and refining augmentation techniques, we anticipate even greater strides in model performance and generalization in future research endeavors. While HVS introduces computational overhead due to its additional forward passes, our findings demonstrate that this overhead is significantly mitigated when using small resolution images in HVS without impeding its performance. This suggests that HVS is likely to continue to outperform baselines regardless of the training length.

¹For completeness, we also experimented with a cooperative HVS (see Appendix F.2 for details).

REFERENCES

- L. Bossard, M. Guillaumin, and L. Van Gool. Food-101 – mining discriminative components with random forests. In *Proc. of ECCV'14*, 2014.
- M. Caron, I. Misra, J. Mairal, P. Goyal, P. Bojanowski, and A. Joulin. Unsupervised learning of visual features by contrasting cluster assignments. In *Proc. of NeurIPS'20*, 2020.
- M. Caron, H. Touvron, I. Misra, H. Jégou, J. Mairal, P. Bojanowski, and A. Joulin. Emerging properties in self-supervised vision transformers. In *Proc. of ICCV'21*, pp. 9630–9640, 2021.
- T. Chen, S. Kornblith, M. Norouzi, and G. E. Hinton. A simple framework for contrastive learning of visual representations. In *Proc. of ICML'20*, pp. 1597–1607, 2020a.
- X. Chen and K. He. Exploring simple siamese representation learning. In *Proc. of CVPR'21*, pp. 15750–15758, 2021.
- Xinlei Chen, Haoqi Fan, Ross B. Girshick, and Kaiming He. Improved baselines with momentum contrastive learning. *CoRR*, abs/2003.04297, 2020b.
- E. Cubuk, B. Zoph, D. Mane, V. Vasudevan, and Q. Le. Autoaugment: Learning augmentation strategies from data. In *Proc. of CVPR'19*, pp. 113–123, 2019.
- J. Deng, W. Dong, R. Socher, L. Li, K. Li, and L. Fei-Fei. ImageNet: A Large-Scale Hierarchical Image Database. In *Proc. of CVPR'09*, pp. 248–255, 2009.
- A. Dosovitskiy, L. Beyer, A. Kolesnikov, D. Weissenborn, X. Zhai, T. Unterthiner, M. Dehghani, M. Minderer, G. Heigold, S. Gelly, J. Uszkoreit, and N. Houlsby. An image is worth 16x16 words: Transformers for image recognition at scale. *arXiv preprint arXiv:12010.11929*, 2020.
- A. Ermolov, A. Siarohin, E. Sangineto, and N. Sebe. Whitening for self-supervised representation learning. In *Proc. of ICML'21*, pp. 3015–3024, 2021.
- M. Everingham, L. Van Gool, C. K. I. Williams, J. M. Winn, and A. Zisserman. The pascal visual object classes (VOC) challenge. In *I. J. of Computer Vision (IJCV'10)*, pp. 303–338, 2010.
- J. Friedman. Greedy function approximation: A gradient boosting machine. *Annals of Statistics*, pp. 1189–1232, 2001.
- J.-B. Grill, F. Strub, F. Altché, C. Tallec, P. H. Richemond, E. Buchatskaya, C. Doersch, B. Ávila Pires, Z. Daniel Guo, M. G. Azar, B. Piot, K. Kavukcuoglu, R. Munos, and M. Valko. Bootstrap your own latent: A new approach to self-supervised learning. In *Proc. of NeurIPS'20*, 2020.
- R. Hadsell, S. Chopra, and Y. LeCun. Dimensionality reduction by learning an invariant mapping. In *Proc. of CVPR'06*, pp. 1735–1742, 2006.
- R. Hataya, J. Zdenek, K. Yoshizoe, and H. Nakayama. Faster autoaugment: Learning augmentation strategies using backpropagation. In *Proc. of ECCV'20*, pp. 1–16, 2020.
- K. He, X. Zhang, S. Ren, and J. Sun. Deep residual learning for image recognition. In *Proc. of CVPR'16*, pp. 770–778, 2016.
- K. He, H. Fan, Y. Wu, S. Xie, and R. B. Girshick. Momentum contrast for unsupervised visual representation learning. In *Proc. of CVPR'20*, pp. 9726–9735, 2020.
- K. He, X. Chen, S. Xie, Y. Li, P. Dollár, and R. B. Girshick. Masked autoencoders are scalable vision learners. In *Proc. of CVPR'22*, pp. 15979–15988, 2022.
- D. Ho, E. Liang, X. Chen, I. Stoica, and P. Abbeel. Population based augmentation: Efficient learning of augmentation policy schedules. In *Proceedings of the 36th International Conference on Machine Learning, ICML 2019, 9-15 June 2019, Long Beach, California, USA*, pp. 2731–2741, 2019.
- C. Hou, J. Zhang, and T. Zhou. When to learn what: Model-adaptive data augmentation curriculum. *CoRR*, abs/2309.04747, 2023.

-
- F. Hutter, H. Hoos, and K. Leyton-Brown. An efficient approach for assessing hyperparameter importance. In *Proc. of ICML'14*, pp. 754–762, 2014.
- iNaturalist 2021 competition dataset. iNaturalist 2021 competition dataset. https://github.com/visipedia/inat_comp/tree/master/2021, 2021.
- M. Jaderberg, K. Simonyan, A. Zisserman, and K. Kavukcuoglu. Spatial transformer networks. In *Proc. of NeurIPS'15*, pp. 2017–2025, 2015.
- A. Krizhevsky. Learning multiple layers of features from tiny images. Technical report, University of Toronto, 2009.
- C. Lin, M. Guo, C. Li, X. Yuan, W. Wu, J. Yan, D. Lin, and W. Ouyang. Online hyper-parameter learning for auto-augmentation strategy. In *Proc. of ICCV'19*, pp. 6578–6587, 2019.
- T.-Y. Lin, M. Maire, S. J. Belongie, J. Hays, P. Perona, D. Ramanan, P. Dollár, and C. L. Zitnick. Microsoft COCO: common objects in context. In *Proc. of ECCV'14*, pp. 740–755, 2014.
- I. Loshchilov and F. Hutter. Decoupled weight decay regularization. In *Proc. of ICLR'19*, 2019.
- S. Müller and F. Hutter. Trivialaugmt: Tuning-free yet state-of-the-art data augmentation. In *Proc. of ICCV'21*, pp. 774–782, 2021.
- M.-E. Nilsback and A. Zisserman. Automated flower classification over a large number of classes. In *Proc. of ICVGIP'08*, pp. 722–729, 2008.
- A. Paszke, S. Gross, F. Massa, A. Lerer, et al. PyTorch: An imperative style, high-performance deep learning library. In *Proc. of NeurIPS'19*, pp. 8024–8035, 2019.
- S. Purushwalkam and A. Gupta. Demystifying contrastive self-supervised learning: Invariances, augmentations and dataset biases. In *Proc. of NeurIPS'20*, 2020.
- S. Ren, K. He, R. B. Girshick, and J. Sun. Faster R-CNN: towards real-time object detection with region proposal networks. In *Proc. of NeurIPS'15*, pp. 91–99, 2015.
- Y. Shi, N. Siddharth, P. H. S. Torr, and A. R. Kosiorek. Adversarial masking for self-supervised learning. In *Proc. of ICML'22*, volume 162, pp. 20026–20040, 2022.
- A. Tamkin, M. Wu, and N. D. Goodman. Viewmaker networks: Learning views for unsupervised representation learning. In *Proc. of ICLR'21*, 2021.
- Y. Tian, D. Krishnan, and P. Isola. Contrastive multiview coding. In *Proc. of ECCV'20*, pp. 776–794, 2020a.
- Y. Tian, C. Sun, B. Poole, D. Krishnan, C. Schmid, and P. Isola. What makes for good views for contrastive learning? In *Proc. of NeurIPS'20*, 2020b.
- A. van den Oord, Y. Li, and O. Vinyals. Representation learning with contrastive predictive coding. *CoRR*, abs/1807.03748, 2018.
- D. Wagner, F. Ferreira, D. Stoll, R. T. Schirrmeister, S. Müller, and F. Hutter. On the importance of hyperparameters and data augmentation for self-supervised learning. *International Conference on Machine Learning (ICML) 2022 Pre-Training Workshop*, 2022.
- M. Wu, C. Zhuang, M. Mosse, D. Yamins, and N. D. Goodman. On mutual information in contrastive learning for visual representations. *arXiv:2005.13149 [cs.CV]*, 2020.
- Yuxin Wu, Alexander Kirillov, Francisco Massa, Wan-Yen Lo, and Ross Girshick. Detectron2. <https://github.com/facebookresearch/detectron2>, 2019.
- Z. Wu, Y. Xiong, S. X. Yu, and D. Lin. Unsupervised feature learning via non-parametric instance-level discrimination. In *Proc. of CVPR'18*, 2018.
- Y. Xing, Q. Song, and G. Cheng. On the algorithmic stability of adversarial training. In *Proc. of NeurIPS'21*, pp. 26523–26535, 2021.

-
- Y. You, I. Gitman, and B. Ginsburg. Large batch training of convolutional networks. *arXiv preprint arXiv:1708.03888*, 2017.
- J. Zbontar, L. Jing, I. Misra, Y. LeCun, and S. Deny. Barlow twins: Self-supervised learning via redundancy reduction. In *Proc. of ICML'21*, pp. 12310–12320, 2021.
- X. Zhang, Q. Wang, J. Zhang, and Z. Zhong. Adversarial AutoAugment. In *Proc. of ICLR'20*, 2020.
- J. Zhou, C. Wei, H. Wang, W. Shen, C. Xie, A. L. Yuille, and T. Kong. ibot: Image BERT pre-training with online tokenizer. *CoRR*, abs/2111.07832, 2021.

APPENDIX A EXAMPLES SAMPLED BY HVS

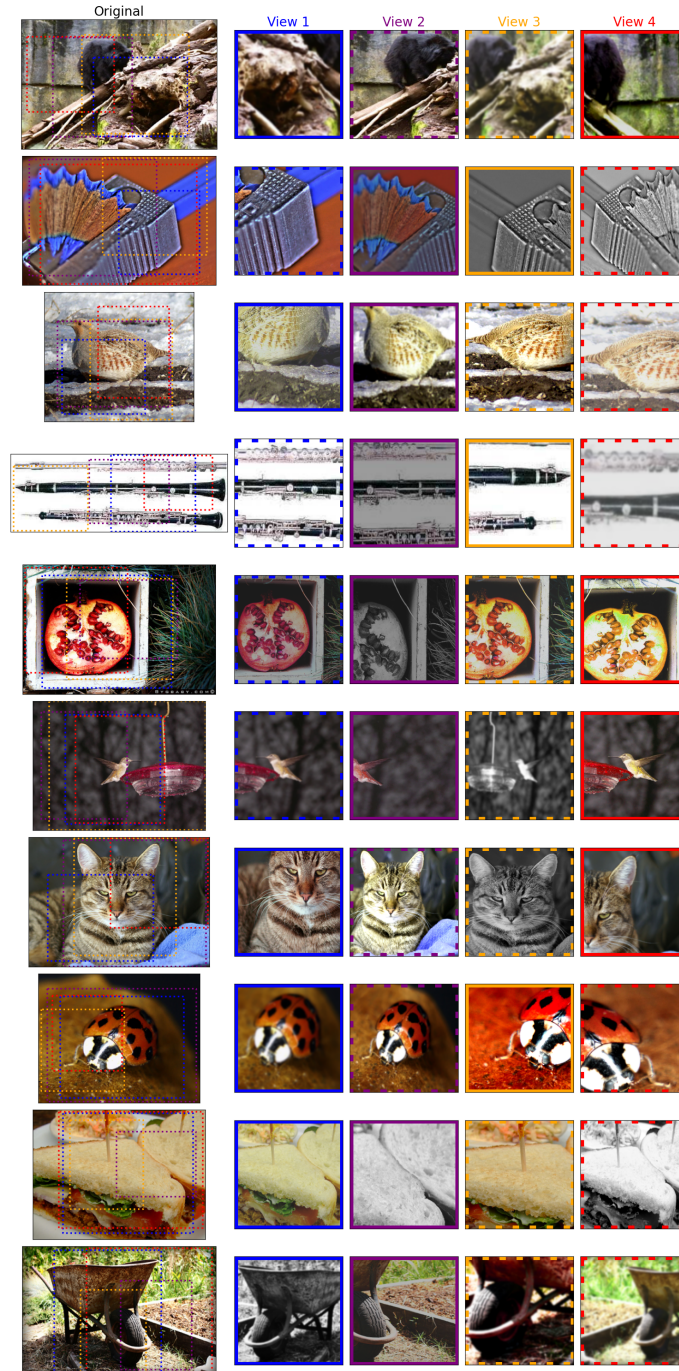


Figure 5: We depict row-wise ten example images from the ImageNet train set along with their sampled views with a finished, 100-epoch trained SimSiam ResNet50 model. Left: original image with the overlaid randomly sampled crops (colored dashed rectangles). Right: All views after applying resizing and appearance augmentations. The pair that is selected adversarially by HVS is highlighted in solid lines, eg. View 1 and View 4 in the first row.

APPENDIX B TRAINING LOSS

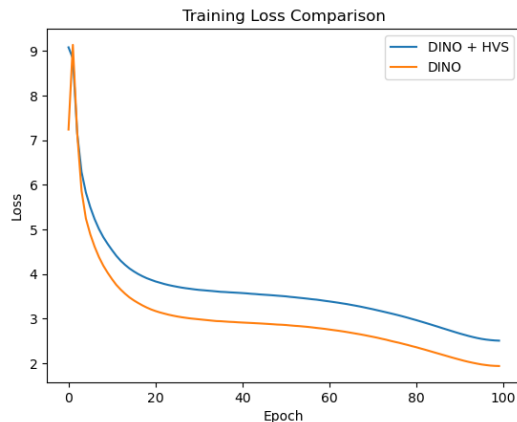


Figure 6: The training loss over 100 epochs. Comparing the DINO vanilla method with DINO + HVS. The spike and drop in the loss curve of DINO is caused by freezing the last layer in the first epoch which was proposed by the authors as a strategy to enhance downstream performance. For HVS we can only see a drop and no spike. We believe this is because HVS exposes the model to hard views from the beginning of training (i.e. the loss is immediately maximized).

APPENDIX C EFFECT OF MORE VIEWS ON LINEAR EVALUATION PERFORMANCE

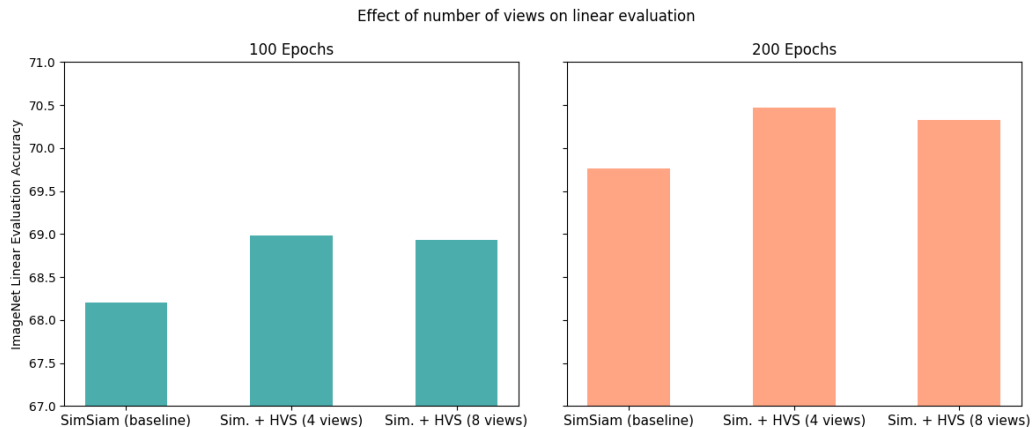


Figure 7: Setting the number of views too high can result in performance deterioration. This shows that diminishing returns exist, likely because the adversary becomes too strong, resulting in a too hard learning task.

APPENDIX D ASSESSING THE IMPORTANCE OF METRICS WITH f ANOVA

To assess the importance of various metrics on the training loss, we apply f ANOVA Hutter et al. (2014) on data that we logged during training with HVS. We used 300k samples that contain the following sampled parameters from the geometric and appearance data augmentation operations for each view: all random resized crop parameters (height and width of the original image, coordinates of crop corners and height and width of the crop), all Colorjitter (color distortion) strengths (brightness, contrast, saturation, hue), grayscale on/off, Gaussian blurring on/off, horizontal flip on/off,

loss, and if the crop was selected or not. The metrics we chose are Intersection over Union (IoU), Relative Distance (sample-wise normalized distance of the center points of crop pairs), color distortion distance (the Euclidean distance between all four color distortion operation parameters, i.e. brightness, contrast, saturation, hue), and the individual color distortion parameters of the Colorjitter operation. As can be seen in Fig. 8, the metric with the highest predictive capacity on the loss is the IoU with an importance of 15.2% followed by brightness with 5.1%. The relative distance has an importance of 3.3%, the colorjitter distance 2.3%, the contrast 1.6%, the saturation 1.4%, hue 0.6%, and all parameters jointly 1.7%.

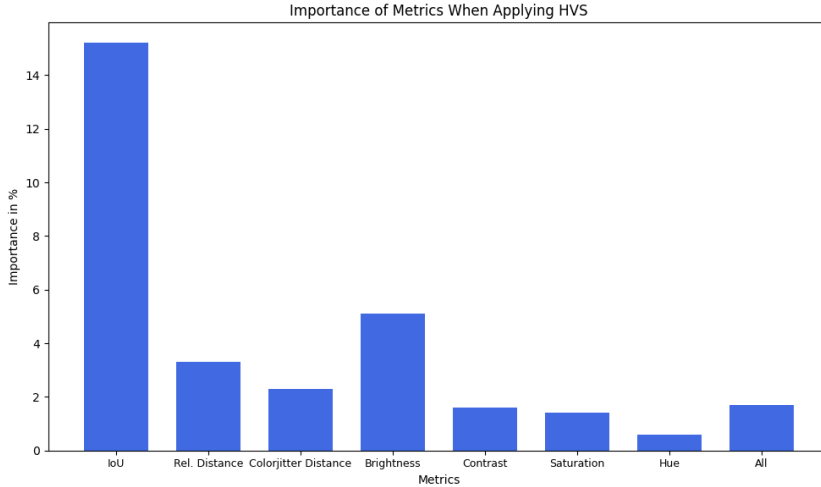


Figure 8: Application of fANOVA Hutter et al. (2014) on logged training data to determine metrics with high predictive capacity on the train loss.

APPENDIX E ADVERSARIAL LEARNER FOR THE VIEW GENERATION

We use Spatial Transformer Network (STN) (Jaderberg et al., 2015) to allow generating views by producing 6D transformation matrices (allowing translating, rotating, shearing, scaling, affine transformations and combinations thereof) in a differentiable way since most common augmentations are not off-the-shelf differentiable. As described, we train it alongside the actual pretrained network using the same (inverted) objective. For our experiments we use DINO with multi-crop, i.e. 2 global and 8 local heads. As STN we use a small CNN with a linear layer for outputting the 10*6D transformation matrices. In this scenario, we use a ViT-tiny/16 with a 300 epoch pretraining on CIFAR10 with a batch size of 256. All other hyperparameters are identical to the ones reported in the DINO paper.

Figure 9 visualizes the procedure. The STN takes the raw image input and generates a number of transformation matrices that are applied to transform the image input into views. These views are then passed to the DINO training pipeline. Both networks are trained jointly with the same loss function. DINO is trained with its original contrastive objective, where the STN is trained by inverting the gradient after the DINO during backpropagation.

As mentioned previously, the STN, without using auxiliary losses, starts zooming in and generating single-color views. To counteract this behavior, we experimented with different penalties on the transformation matrices produced by the STN. For instance, in order to limit the zooming pattern, we can use the determinants of the sub-matrices of the transformation matrix to penalize based on the area calculated and apply a regression loss (e.g. MSE). We refer to this type of penalty as *Theta Crops Penalty* (TCP). Additionally, we also restrict its parameters to stay within a sphere with different parameters for local and global crops. Next to determinant-based penalty losses, we also experimented with other penalty functions such as the weighted MSE between the identity and the current transformation matrix or penalties based on histograms of the input image and generated views after applying the transformation. To avoid strong uni-dimensional scaling behavior, we

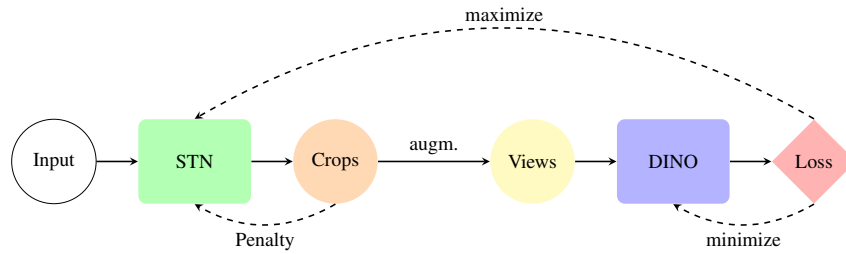


Figure 9: Illustration of adversarial learning with a Spatial Transformer Network (STN) jointly with contrastive learning (here: DINO).

also implemented restricting scaling in a symmetric way (i.e. applied to both x and y dimensions) and refer to this as *scale-sym.*. We report our best results in Table 6 which are all TCP-based. As can be seen, no setting is able to outperform the baseline. Our best score was achieved with translation-scale-symmetric which is very similar to random cropping. When removing the symmetries in scaling, the performance drops further. Removing a constraint adds one transformation parameter and therefore one dimension. This can be seen as giving more capacity to the adversarial learner which in turn can make the task significantly harder. Similarly, when adding rotation, the performance drops further and in part drastically. This is on the one hand due to the penalties not being fully able to restrict the output of the STN. On the other, the task of extracting useful information from two differently rotated crops is even harder, and learning spatial invariance becomes too challenging. All in all, we experienced two modes: either the STN is too restricted, leading to *static output* (i.e. independent of image content, the STN would produce constant transformation matrices) or the STN has too much freedom, resulting in extremely difficult tasks. See Fig. 10 for an example on the former behavior.



Figure 10: Example for static output behavior of the STN.

Mode	Penalty	Lin.	F.T.
baseline	-	86.1	92.7
translation-scale-sym.	TCP	83.7	90.3
translation-scale	TCP	82.8	89.7
rotation-translation	TCP	56.7	-
rotation-translation-scale	TCP	31.7	-
rotation-translation-scale-sym.	TCP	77.6	-
affine	TCP	78.3	83.5

Table 6: **Linear evaluation and finetuning classification performance on CIFAR10.** Top-1 accuracy on the validation set of CIFAR10 for our best results reported with different STN transformation modes.

APPENDIX F ADDITIONAL RESULTS

F.1 OBJECT DETECTION AND INSTANCE SEGMENTATION

For our object detection and instance segmentation analysis experiment, we report additional results in Table F.1 based on the AP metric. We use the C4 backbone variant (Wu et al., 2019) and finetuning with the 1x schedule.

Method	Arch.	VOC07+12 Object Det.			COCO Instance Segm.		
		AP _{all}	AP ₅₀	AP ₇₅	AP _{mask}	AP _{mask50}	AP _{mask75}
SimSiam	RN50	52.05	78.46	56.88	27.16	45.16	28.48
+ HVS	RN50	52.91	79.06	57.55	27.93	46.51	29.36
Improvement		+0.86	+0.60	+0.67	+0.77	+1.35	+0.88
DINO	RN50	53.66	80.86	58.60	30.25	50.35	31.78
+ HVS	RN50	52.86	80.51	58.21	30.02	50.39	31.52
Improvement		+0.80	-0.36	-0.39	-0.23	+0.04	-0.27

Table 7:

F.2 EASY VIEW SELECTION

To investigate the effect of a *cooperative*, i.e. easy pair selection, we conducted a small experiment. Instead of selecting the pair yielding the worst loss, we inverted the objective and selected the pair with the best loss. As expected, this led to model collapses with a linear eval. performance of 0.1%. This result is in line with previous findings that highlight the importance of strong augmentations in CL.

APPENDIX G HYPERPARAMETERS

G.1 EVALUATIONS ON IMAGENET

G.1.1 DINO

For DINO, we report the ViT pretraining hyperparameters in Table 8. For ResNet-50, we use the same hyperparameters. Note, for HVS we limit the total number of comparisons to 128 across all heads. Linear evaluation is executed for 100 epochs and we use a learning rate of 0.001, SGD optimizer (AdamW (Loshchilov & Hutter, 2019) during pretraining), a batch size of 1024, a momentum of 0.9, and no weight decay.

G.1.2 SIMSIAM

In Table 9, we report the ResNet-50 pretraining hyperparameters. Linear evaluation is executed for 90 epochs (as reported by the SimSiam authors) and we use a learning rate of 0.1, LARS optimizer (You et al., 2017), a batch size of 4096, and no weight decay.

G.1.3 SIMCLR

We report the ResNet-50 pretraining hyperparameters for SimCLR in Table 10. Linear evaluation is executed for 90 epochs with a learning rate 0.1, SGD optimizer, batch size of 4096 and no weight decay.

Hyperparameter	Value	Hyperparameter	Value
architecture	vit_small	epochs:	100
img_size	224	warmup_epochs:	10
patch_size	16	freeze_last_layer:	1
out_dim	65536	lr:	0.0005
norm_last_layer	true	min_lr:	1.0e-06
momentum_teacher	0.996	optimizer:	AdamW
use_bn_in_head	false	weight_decay:	0.04
teacher_temp	0.04	weight_decay_end:	0.4
warmup_teacher_temp	0.04	global_crops_scale:	0.4, 1.0
warmup_teacher_temp_epochs	0	global_crops_size:	224
fp16	true	local_crops_number:	8
batch_size	512	local_crops_scale	0.05, 0.4
clip_grad	3.0	local_crops_size:	96
drop_path_rate	0.1		

Table 8: Pretraining ImageNet hyperparameters for the runs with DINO. For 300 epochs, we use a batch size of 1024.

Hyperparameter	Value
architecture	resnet50
batch_size	512
blur_prob	0.5
crops_scale	0.2, 1.0
crop_size	224
feature_dimension	2048
epochs	100
fix_pred_lr	true
lr	0.05
momentum	0.9
predictor_dimension	512
weight_decay	0.0001
optimizer	SGD

Table 9: Pretraining ImageNet hyperparameters for the runs with SimSiam. For 300 epochs, we use a batch size of 1024.

Hyperparameter	Value
architecture	resnet50
proj_hidden_dim	2048
out_dim	128
use_bn_in_head	true
batch_size	4096
optim	LARS
lr	0.3
sqrt_lr	false
momentum	0.9
weight_decay	1e-4
epochs	100
warmup_epochs	10
zero_init_residual	true

Table 10:

G.2 TRANSFER TO OTHER DATASETS AND TASKS

For linear evaluation on the transfer datasets, we simply used the same hyperparameters for linear evaluation on ImageNet (DINO and SimSiam respectively). For finetuning DINO ViT-S/16, we used the hyperparameters reported in Table 11 and for SimSiam ResNet-50 we used the hyperparameters in Table 12

Hyperparameter	CIFAR10	CIFAR100	Flowers102	iNat 21	Food101
lr	7.5e-6	7.5e-6	5e-5	5e-5	5e-5
weight_decay	0.05	0.05	0.05	0.05	0.05
optimizer	AdamW	AdamW	AdamW	AdamW	AdamW
epochs	300	300	300	100	100
batch_size	512	512	512	512	512

Table 11: Finetuning hyperparameters for DINO ViT-S/16.

Hyperparameter	CIFAR10	CIFAR100	Flowers102	iNat 21	Food101
lr	7.5e-6	5e-6	5e-4	7e-5	5e-6
weight_decay	0.05	0.05	0.05	0.05	0.05
optimizer	AdamW	AdamW	AdamW	AdamW	AdamW
epochs	300	300	300	100	100
batch_size	512	512	512	512	512

Table 12: Finetuning hyperparameters for SimSiam and ResNet-50.

G.3 OBJECT DETECTION AND INSTANCE SEGMENTATION

We have used the Detectron2 library (Wu et al., 2019) for object detection and instance segmentation. We followed the public codebase from MoCo (He et al., 2020) (like SimSiam) for all entries. Due to limited compute resources we changed the batch size. All parameters that differ from MoCo are reported in the Table 13. The pretrained models are finetuned end-to-end on the target datasets. All methods are based on 100-epoch pre-training on ImageNet.

	VOC07+12 Object Det.	Cocoe Inst. Segm.
Hyperparameter	Value	Value
batch_size	8	8
lr	0.01	0.01
steps	48000	90000

Table 13: Hyperparameters for VOC object detection and COCO instance segmentation.

APPENDIX H COMPUTATIONAL OVERHEAD OF HVS

In Table 14, we compare the computational overhead factors across multiple baselines. The details of hardware and software used for this analysis are: NVIDIA RTX 3080, AMD R7 5800X, 32GB RAM, Ubuntu 22.04, PyTorch 2.0.1, CUDA 11.8. For DINO’s 2 global and 8 local views (default), applying HVS with nviews=2 sampled for each original view results in 4 global and 16 local views. Since considering all combinations would yield over 77k unique comparisons (4 over 2 times 16 over 8), to remain tractable, we limit the number of total comparisons to 128. Overall, reducing the image resolution can significantly reduce the time complexity of HVS. For instance, in the case of DINO ViT-S/16, the reduction leads to approximately 30% faster training times and as reported in the main paper, a 50% reduction allows retaining original performance.

Res.	SimSiam (RN50)	DINO (ViT)
100%	x1.55	x2.15
75%	x1.45	x1.68
50%	x1.24	x1.56
25%	x1.16	x1.5

Table 14: Time slowdown factors under different image resolutions for the selection in HVS.

While technically there can be a memory overhead with HVS, with the number of sampled views chosen in this paper, the backward pass of the methods that compute gradients only for the selected view pair still consumes more memory than the selection part of HVS (even for 8 sampled views in SimSiam). Note, that selection and the backward computation are never executed at the same time but sequentially.

We emphasize that the time overhead factors were measured without any optimization of HVS’ efficiency and, in our view, there are multiple ways to improve it. In our work, we opted for the easiest implementation possible to showcase that selecting harder views dependent on the model learning state can help boost performance in contrastive learning. Going forward with more compute-efficient HVS solutions, one could think of:

- using embeddings of views from “earlier” layers in the networks or
- using 4/8 bit low-precision for the view selection or
- using one GPU just for creating embeddings and selecting the hardest views while the remaining GPUs are used for learning or
- switching between HVS and the standard pipeline in alternating fashion or
- bypassing forwarding of similar pairs and more

APPENDIX I HARD VIEW SELECTION OBJECTIVES

I.1 SIMCLR

In this section, we are going to introduce the application of HVS with the SimCLR objective. Assume a given set of images \mathcal{D} , an image augmentation distribution \mathcal{T} , a minibatch of M images $\mathbf{x} = \{x_i\}_{i=1}^M$ sampled uniformly from \mathcal{D} , and two sets of randomly sampled image augmentations $A = \{t_i \sim \mathcal{T}\}_{i=1}^M$ and B sampled from \mathcal{T} . We apply A and B to each image in \mathbf{x} resulting in \mathbf{x}^A and \mathbf{x}^B . Both augmented sets of views are subsequently projected into an embedding space with $\mathbf{z}^A = g_\theta(f_\theta(\mathbf{x}^A))$ and $\mathbf{z}^B = g_\theta(f_\theta(\mathbf{x}^B))$ where f_θ represents an encoder (or backbone) and g_θ a projector network. Contrastive learning algorithms then minimize the following objective function:

$$\mathcal{L}(\mathcal{T}, \mathbf{x}; \theta) = -\log \frac{\exp(\text{sim}(\mathbf{z}_i^A, \mathbf{z}_i^B)/\tau)}{\sum_{i \neq j} \exp(\text{sim}(\mathbf{z}_i^A, \mathbf{z}_j^B)/\tau)} \quad (3)$$

where τ denotes a temperature parameter and *sim* a similarity function that is often chosen as cosine similarity. Intuitively, when optimizing θ , embeddings of two augmented views of the same image are attracted to each other while embeddings of different images are pushed further away from each other.

To further enhance the training process, we introduce a modification to the loss function where instead of having two sets of augmentations A and B , we now have “N” sets of augmentations, denoted as $\mathcal{A} = \{A_1, A_2, \dots, A_N\}$. Each set A_i is sampled from the image augmentation distribution \mathcal{T} , and applied to each image in \mathbf{x} , resulting in “N” augmented sets of views $\mathbf{x}^{A_1}, \mathbf{x}^{A_2}, \dots, \mathbf{x}^{A_N}$.

Similarly, we obtain N sets of embeddings $\mathbf{z}^{A_1}, \mathbf{z}^{A_2}, \dots, \mathbf{z}^{A_N}$ through the encoder and projector networks defined as:

$$\mathbf{z}^{A_i} = g_\theta(f_\theta(\mathbf{x}^{A_i})), \quad i = 1, 2, \dots, N$$

We then define a new objective function that seeks to find the pair of augmented images that yield the highest loss. The modified loss function is defined as:

$$\mathcal{L}_{\max}(\mathcal{T}, \mathbf{x}; \theta) = \max_{k, l: k \neq l} \mathcal{L}(\mathcal{T}, \mathbf{x}; \theta)_{kl}$$

where

$$\mathcal{L}(\mathcal{T}, \mathbf{x}; \theta)_{kl} = -\log \frac{\exp(\text{sim}(\mathbf{z}_k^{A_k}, \mathbf{z}_k^{A_l})/\tau)}{\sum_{i \neq j} \exp(\text{sim}(\mathbf{z}_i^{A_k}, \mathbf{z}_j^{A_l})/\tau)}$$

and $k, l \in \{1, 2, \dots, N\}$ and $i, j \in \{1, 2, \dots, M\}$.

For each iteration, we evaluate all possible view pairs and contrast each view against every other example in the mini-batch. Intuitively, the pair that yields the highest loss is selected, which is the pair that at the same time minimizes the numerator and maximizes the denominator in the above equation. In other words, the hardest pair is the one, that has the lowest similarity with another augmented view of itself and the lowest dissimilarity with all other examples.

APPENDIX J ATTENTION MAPS

In this section, we visualize attention maps as a way to qualitatively study the potential effects and differences of the HVS learning method and their resulting features. The provided attention maps are from a DINO ViT-S/16 100 model, and we contrast the attention for each HVS and the baseline. All input images are from the ImageNet-1k validation split. The color code used depicts strong attention in yellow and weak attention in green and attentions from the HVS model are shown in the top row and attentions from the baseline in the bottom row, respectively. To summarize this study, we do not see apparent strong differences between HVS and the baseline. What we occasionally notice is that the HVS models seem to capture the shape of some subtle/indistinct objects better (e.g. the creek/river in the valley in Fig. 12, the lizard in Fig. 13, or the speaker in Fig. 14 or focus slightly more on the context and background (Fig. 16, 17, and 18).

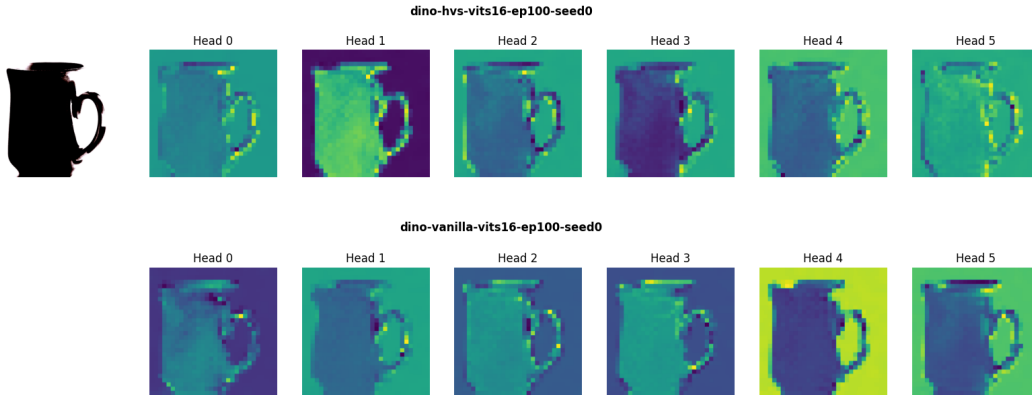


Figure 11:

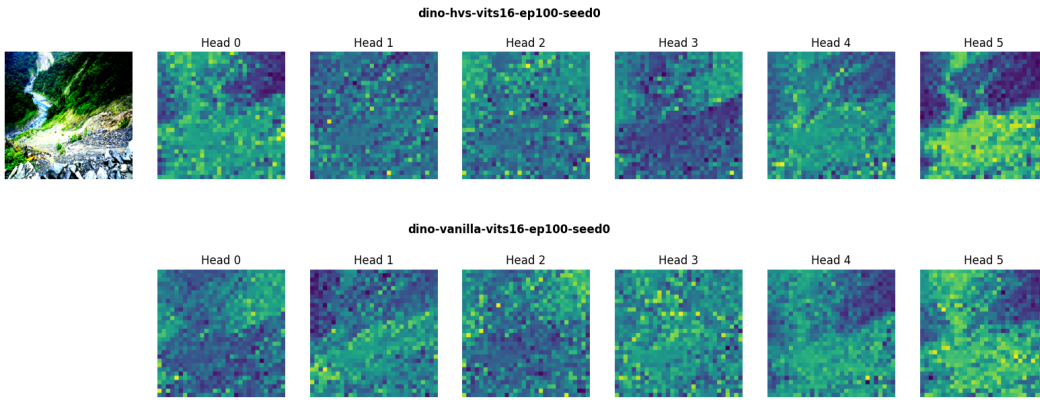


Figure 12:

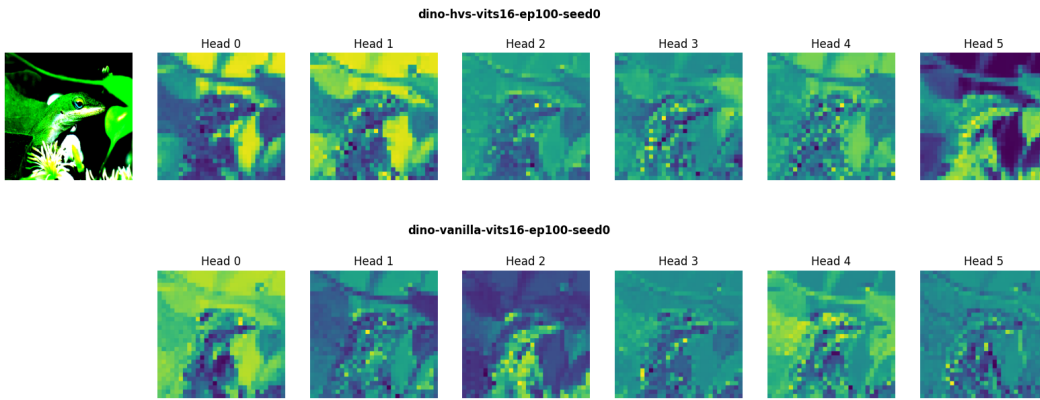


Figure 13:

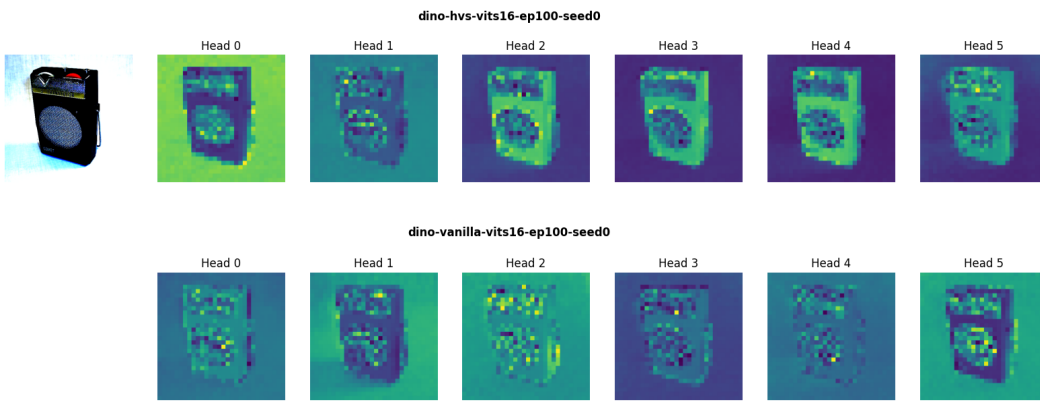


Figure 14:

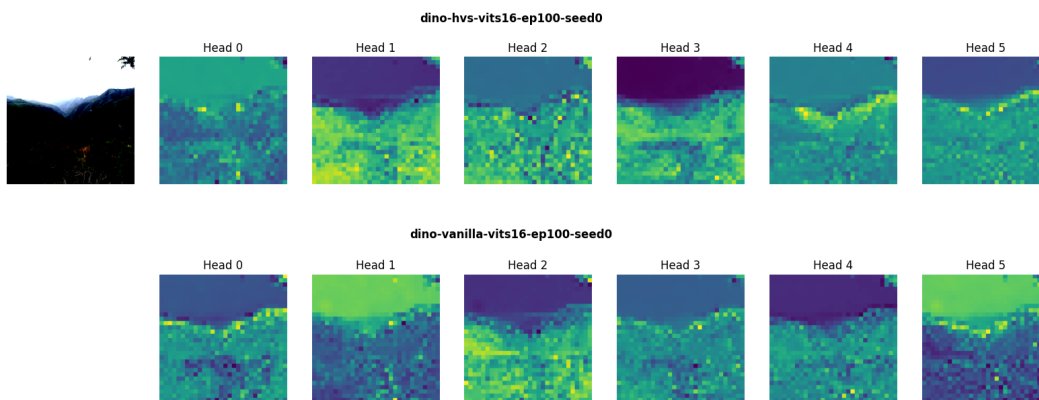


Figure 15:

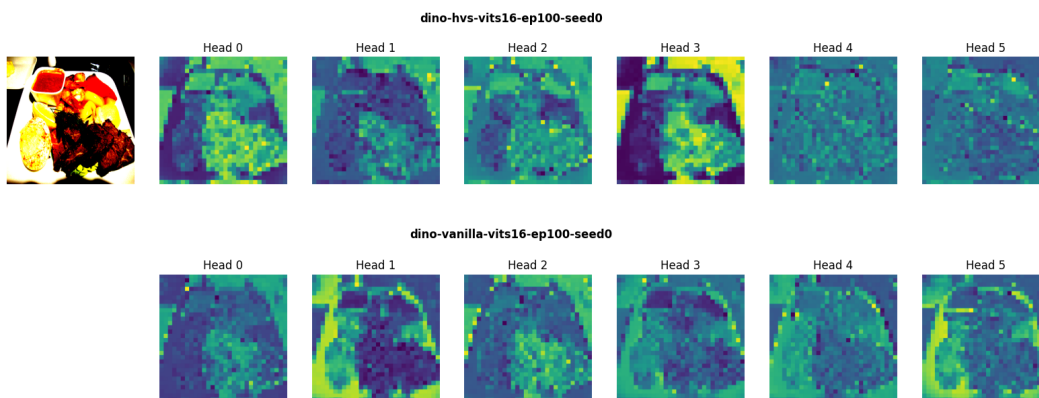


Figure 16:

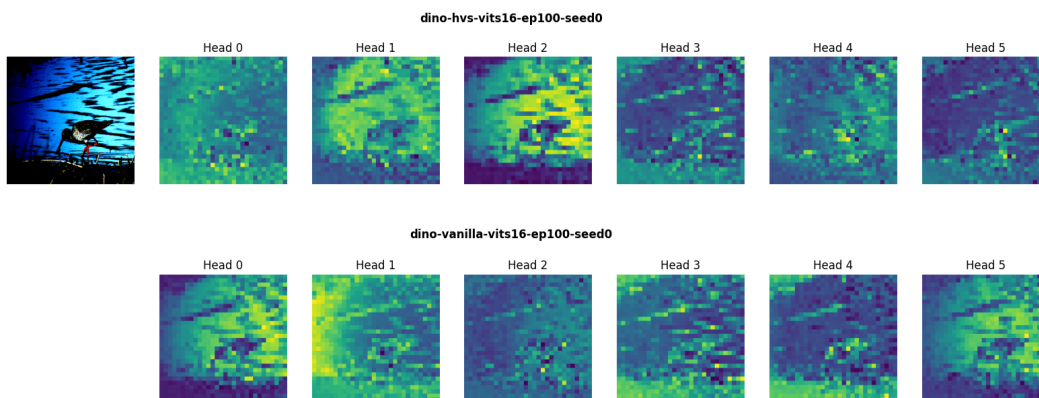


Figure 17:

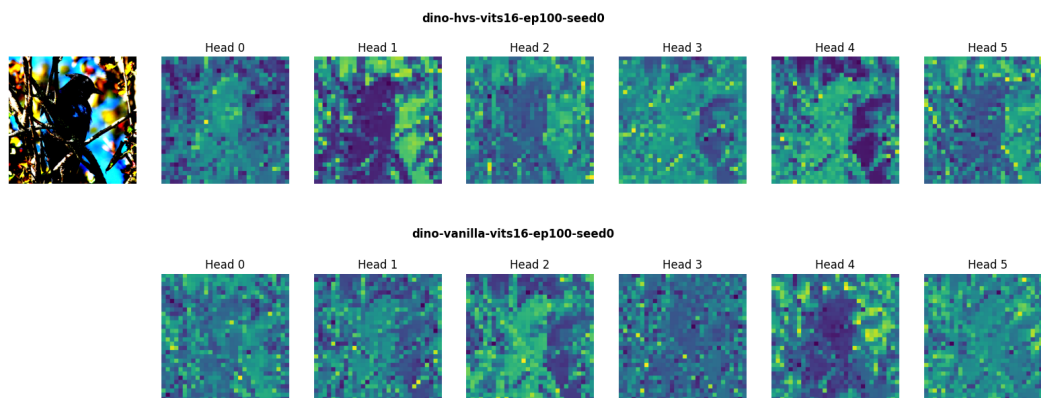


Figure 18:

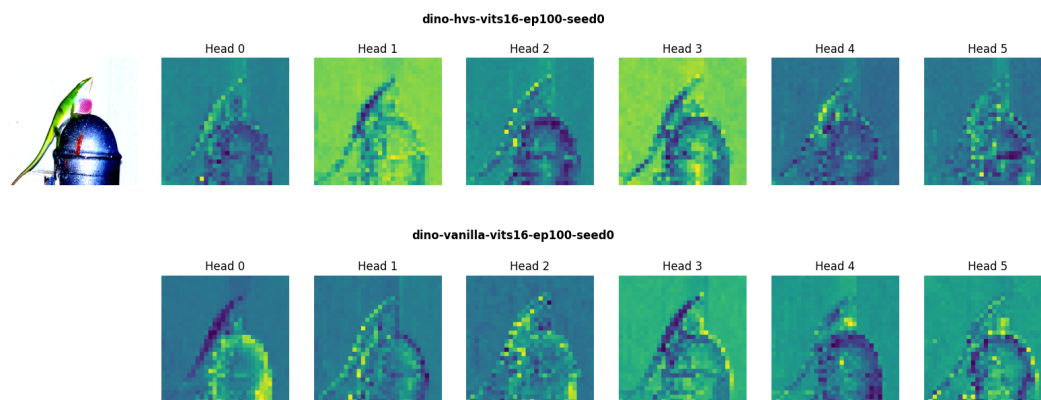


Figure 19: